SPECIAL
DYNAMO/CINDY/AMIE/LASP
COLLECTION

A Lagrangian View of Moisture Dynamics during DYNAMO

WALTER M. HANNAH

Department of Marine, Earth, and Atmospheric Sciences, North Carolina State University, Raleigh, Raleigh, North Carolina

BRIAN E. MAPES

Department of Atmospheric Sciences, Rosenstiel School of Marine and Atmospheric Science, University of Miami, Miami, Florida

GREGORY S. ELSAESSER

NASA Goddard Institute for Space Studies, Columbia University, New York, New York

(Manuscript received 17 August 2015, in final form 12 November 2015)

ABSTRACT

Column water vapor (CWV) is studied using data from the Dynamics of the Madden–Julian Oscillation (DYNAMO) field experiment. A distinctive moist mode in tropical CWV probability distributions motivates the work. The Lagrangian CWV tendency (LCT) leaves together the compensating tendencies from phase change and vertical advection, quantities that cannot be measured accurately by themselves, to emphasize their small residual, which governs evolution. The slope of LCT versus CWV suggests that the combined effects of phase changes and vertical advection act as a robust positive feedback on CWV variations, while evaporation adds a broadscale positive tendency. Analyzed diabatic heating profiles become deeper and stronger as CWV increases. Stratiform heating is found to accompany Lagrangian drying at high CWV, but its association with deep convection makes the mean LCT positive at high CWV. Lower-tropospheric wind convergence is found in high-CWV air masses, acting to shrink their area in time. When ECMWF heating profile indices and S-Pol and TRMM radar data are binned jointly by CWV and LCT, bottom-heavy heating associated with shallow and congestus convection is found in columns transitioning through Lagrangian moistening into the humid, high-rain-rate mode of the CWV distribution near 50–55 mm, while nonraining columns and columns with widespread stratiform precipitation are preferentially associated with Lagrangian drying. Interpolated sounding-array data produce substantial errors in LCT budgets, because horizontal advection is inaccurate without satellite input to constrain horizontal gradients.

1. Introduction

The Madden–Julian oscillation (MJO) is characterized by alternating intraseasonal periods of anomalous rain and wind in the tropical Indian and west Pacific Ocean regions (Madden and Julian 1972; Zhang 2005). It stands apart from the better-understood spectrum of convectively coupled waves (CCW) in the tropical troposphere, and understanding the MJO has been called the "holy grail" of tropical meteorology (Raymond 2001). To gather data on MJO initiation, a recent international field campaign called DYNAMO/CINDY/AMIE 2011,[1] herein DYNAMO, was conducted in 2011/12 in the sparsely observed region of the equatorial Indian Ocean (Yoneyama et al. 2013; Johnson and Ciesielski 2013; Zhang et al. 2013). This paper describes efforts flowing from that field campaign.

Ordinary CCWs are thought to arise from a nearly linear coupling between deep convection and nearly adiabatic vertical displacements of background stratification

Corresponding author address: Walter M. Hannah, Department of Marine, Earth, and Atmospheric Sciences, North Carolina State University, Campus Box 8208, Raleigh, NC 27695.
E-mail: walter@hannahlab.org

[1] Acronyms for Dynamics of the MJO, Cooperative Indian Ocean Experiment on Intraseasonal Variability in Year 2011, and ARM MJO Investigation Experiment.

DOI: 10.1175/JAS-D-15-0243.1

© 2016 American Meteorological Society

Brought to you by NOAA Central Library | Unauthenticated | Downloaded 08/13/24 01:21 PM UTC

by wave motions, which exhibit a vertical dipole of vertical velocity [vertical wavenumber 1; see review by Kiladis et al. (2009)]. Deep convective cloud systems have a bottom-heavy profile of sensitivity to their environment but produce a top-heavy profile of heating owing to associated stratiform precipitation (Houze 1997), reexciting the dipole mode in the same phase that triggers convective systems. The resulting instability of wave periods much longer than a convection–stratiform transition time is called "stratiform instability" for that reason (Mapes 2000). Modulation of convection's depth by midlevel moisture is also implicated in this instability of vertical wavenumber 1 (Kuang 2008).

The MJO is thought to have fundamentally different dynamics from such CCWs for several reasons. First, its propagation does not fall along linear dispersion curves characteristic of the dipole wave mode in the equatorial region, and its propagation speed is so slow that advection by observed winds, both mean and MJO-variable anomalies, cannot be neglected. Second, the ratio of anomalous water vapor mixing ratio q_v to dry static energy s is much greater than that of CCWs and far greater than the ratio of vertical gradients dq/dp to ds/dp that would characterize adiabatic vertical displacements of ambient stratification (Mapes et al. 2006). Apparently moisture in the MJO is modulated in more complex, presumably cloud population mediated, ways.

The MJO's relatively large amplitude in moisture, and the emergence of new low-frequency solutions in relevant equation sets when a moisture variable is included ("moisture modes"; e.g., Sobel et al. 2001; Raymond and Fuchs 2009; Sugiyama 2009; Adames and Kim 2016), has led to the view that vertical storage and horizontal transport of moisture are uniquely essential mechanisms in the MJO. A parallel literature on column-integrated moist static energy, which is almost equivalent to column water vapor (CWV) since tropical temperature is so nearly constant (Charney 1963), also plays into a moisture-centric view of MJO dynamics (Maloney 2009; Andersen and Kuang 2012; Hannah and Maloney 2014).

While moisture changes may be essential to the MJO, straightforward budget evaluations are vexed by the fact that any one of several terms, or slight shifts in the imbalances among them, could suffice to explain MJO-related time changes; and by the same token, errors of many kinds may suffice to thwart the effort (Tseng et al. 2015). Precision can be gained by averaging over large space–time regions, but the picture becomes ever blurrier, and causality ever hazier. For example, on the local scale (~25 km), the relationship between CWV and precipitation is known to be strikingly nonlinear, almost steplike, with a critical value near 75% of column saturation or about 50-mm liquid equivalent in CWV (Bretherton et al. 2004; Sahany et al. 2012). The broader scales and long lifetime of CWV features compared to spotty convective precipitation fields (e.g., http://tropic.ssec.wisc.edu/real-time/mimic-tpw/global2/main.html) implies that this association is not a tautology of convective updrafts saturating the exact columns they occupy but, rather, a modulation of the probability-of-convection field on scales of hundreds to thousands of kilometers by patches and filaments of the long-lived CWV field. Given such a nonlinear relationship, bulk space–time averages of CWV (the argument to the nonlinear function) would seem to be a poor approach, even if CWV is indeed a key variable in the causal chain.

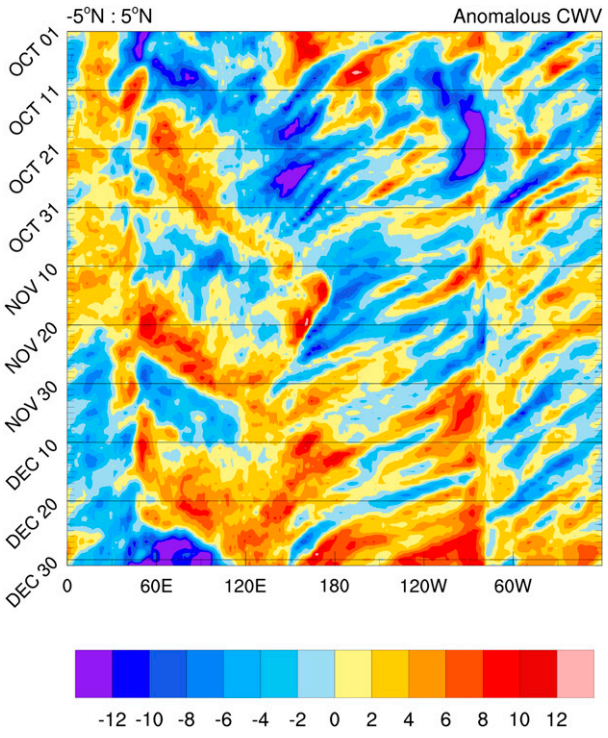

FIG. 1. Hovmöller diagrams of tropical column water vapor anomalies (millimeters of liquid equivalent; kg m^{-2}) from ECMWF analysis during October–December 2011 latitudinally averaged over 5°S–5°N.

For these reasons, we focus here on a space–time-resolved (on 6 hourly and 0.25° grids) view of the CWV field within the DYNAMO MJO events, emphasizing processes that take air columns across and around the critical value of CWV for the nonlinear pickup in precipitation, which we shall see is also near a distinct mode in CWV's frequency distribution. Such a column-by-column view may then be spatially aggregated up, which we hope will inform considerations of MJO dynamics more effectively than bulk-averaged moisture budgets of large regions.

Coherent variations in CWV were indeed observed in the DYNAMO period. Figure 1 shows a time–longitude diagram of temporal anomalies of CWV averaged from

Brought to you by NOAA Central Library | Unauthenticated | Downloaded 08/13/24 01:21 PM UTC

5°S to 5°N during October–December 2011 from ECMWF analyses. DYNAMO's three prominent MJO events are seen in the Indian Ocean (red streaks in left side of Fig. 1), along with smaller-scale westward-moving features in the easterlies across the Pacific and Atlantic sectors. Budget studies have shown that large-scale horizontal advection is one of the leading processes driving the moisture variability associated with the MJO (Maloney 2009; Kiranmayi and Maloney 2011; Sobel and Maloney 2013; Andersen and Kuang 2012; Sobel et al. 2014). Water vapor tendencies by vertical advection and condensation are both much larger in magnitude, but these processes are tightly coupled and largely cancel, leaving a residual moisture tendency that is comparable to the horizontal advection (Chikira 2014).

Column-integrated water vapor is well measured by microwave radiometry, over the oceans from a robust constellation of satellites, and from the surface anywhere by microwave radiometry or even by low-cost GPS-meteorology equipment (Adams et al. 2015). This makes it an especially attractive quantity to study observationally. Theoretical considerations arguably militate for studying column moist static energy instead, but in practice these quantities are almost exactly proportional in our equatorial domain (as discussed further below). In this study we characterize moistening and drying processes during DYNAMO, without separating the effects of phase changes and vertical advection. To do this, we use a nominally Lagrangian framing of the CWV budget, in which the instantaneous net moistening of a moving Lagrangian column or 0.25°-scale air mass is diagnosed by estimating the budget's left-hand side.

Physically, we wish to know the following:

1) Does the Lagrangian CWV tendency (LCT) provide a positive or negative feedback on CWV?
2) Are certain cloud types associated with certain LCT values?

As a practical matter for future field-campaign strategies, we will also evaluate the following:

3) How well is the LCT estimated with sounding-array data alone?

Section 2 provides a mathematical derivation of the LCT. Descriptions of data used in our analysis are given in section 3. Comparison of the LCT in analysis and sounding data is presented in section 4, followed by analysis of radar data in the context of the LCT in section 5. Summary and conclusions are discussed in section 6.

2. Framework: The Lagrangian tendency of CWV

The Eulerian budget of water vapor in advective form, in a hydrostatic pressure coordinate, integrated over column mass as indicated by angle brackets, may be written as follows:

$$\langle \partial_t q_v \rangle + \langle \mathbf{v} \cdot \nabla q_v \rangle + \langle \omega \partial_p q_v \rangle = E - P, \tag{1}$$

where q_v is specific humidity, $\mathbf{v}$ is the horizontal wind vector, ω is the vertical pressure velocity, and the column integral of evaporation minus condensation is the surface evaporation minus surface precipitation ($E - P$).

Several problems typically arise when directly estimating the terms of (1) from observations. Evaporation E is reasonably estimated from a simple from a bulk formula, but P is very fine grained and skewed, which makes in situ observations hard to generalize over area, while satellite retrievals are limited by a number of factors (Krajewski and Smith 2002; Kidd and Huffman 2011). Vertical velocity is also fine grained and skewed and is measurable only indirectly as horizontal wind divergence over a large area. In practice, that divergence estimate is subjected to large corrections, with precipitation as an auxiliary input variable (Zhang et al. 1999). The difference between sink P and the source by vertical advection would be lost in the noise of observations and retrievals of the two quantities separately.

In light of these difficulties, let us instead recast the budget to describe the horizontally LCT,

$$\langle \partial_t q_v \rangle + \langle \mathbf{v} \cdot \nabla q_v \rangle = -\langle \omega \partial_p q_v \rangle + E - P$$
$$\frac{D\langle q_v \rangle}{Dt} = \mathrm{LCT}, \tag{2}$$

which describes the net moistening of an air column. The left-hand side is the difference of the local Eulerian and horizontal advective tendencies. If horizontal advection were the only process affecting a 2D conserved quantity $\langle q_v \rangle$ = CWV, then these terms would exactly cancel, and (2) = 0. The right-hand side accounts for the net moistening by various processes within a moving column of air. This could also be called the vertically integrated "column process," which represents all processes acting in the vertical (Chikira 2014).

The advantage of this perspective is that we can estimate the right-hand side not through error-prone estimates of its largely canceling individual terms[2] but, rather, by constructing the left-hand side of (2) that only involves the profile of water vapor and horizontal wind, quantities that are better constrained by observations than precipitation and vertical velocity.

[2] Cancellation is especially large between P and advection by vertical motions driven by its associated latent and radiative heatings. Evaporation E depends mainly on wind speed and is less problematic to estimate.

Brought to you by NOAA Central Library | Unauthenticated | Downloaded 08/13/24 01:21 PM UTC

Why not eliminate precipitation in (2) by analyzing a budget of moist static energy (MSE) like many other studies? A similar rearrangement of the column MSE budget yields a budget with only radiative heating and net surface fluxes as source terms on the rhs, both of which are observationally tractable quantities. However, vertical MSE advection remains problematic to estimate given the uncertainties of vertical velocity. Recasting that as horizontal flux convergence helps a little, since Gauss's integral theorem can then be used to build ''gross'' (area averaged) estimates. Still, this integral hinges on subtle features of the vertical profiles of the divergent component of the analyzed wind which are much more error prone than the total horizontal advection in (2).

In practice, column MSE budget analysis often treats vertical advection term as a target of estimation rather than a tool. A normalized form of this term has been given the moniker ''gross moist stability'' (GMS; Neelin and Held 1987; Raymond et al. 2009). The value of GMS depends on scale (the adjective gross being loosely defined) and, furthermore, characterizes a moist flow phenomenon as a whole (a mixture of its dynamic and thermodynamic fields). It is not a property of a background state for such phenomena, like other quantities bearing the name ''stability,'' and is not expected even theoretically to have a universal value. The endpoint of MSE budget literature thus seems to be a confounding range of values for an abstract quantity that is only as well defined as the adjective gross and is, arguably, misleadingly named. Still, the results of such studies are related to, and necessarily consistent with, our results below, since fluctuations of column MSE and q_v are almost exactly equal in the equatorial belt, where column temperature fluctuations are small. For instance, the 20-mm range of Fig. 1 corresponds to about 8 K in MSE units—far larger than any observed tropical column temperature variations. For these reasons, here we confine ourselves to the relatively straightforward business of the moisture budget at 0.25° and 6-hourly scales.

3. Data sources

The analysis reported here utilized several data sources. Gridded humidity and wind data for budget calculations are taken from the European Centre for Medium-Range Weather Forecasts (ECMWF) operational analysis and also from the CSU interpolated analysis of the DYNAMO large-scale sounding array (Johnson and Ciesielski 2013; Yoneyama et al. 2013; Ciesielski et al. 2014). The ECMWF data are 6 hourly on a 0.25° grid, whereas the sounding datasets are 3 hourly on a 1° grid. There are several versions of sounding dataset available, but this study mainly uses version 2b, which incorporates some ECMWF analysis. Using version 2a (no ECMWF analysis) does not substantially change the results, unless noted in the text. At the time of this writing, versions 3a and 3b became available. However, the update only addressed minor issues in the surface temperature and humidity measurements in the southern sounding array and is, therefore, not relevant to the results presented here.

Several remote sensing datasets were analyzed in this study. Satellite-derived CWV was obtained from the Morphed Integrated Microwave Imagery at CIMSS (MIMIC) gridded data product (Wimmers and Velden 2011). Data from a radiometer located on Gan Island are used for a localized comparison of CWV datasets. The radiometer values were obtained using a statistical retrieval whose coefficients were determined from the historical Gan radiosonde dataset, but rain-contaminated samples have not yet been eliminated (P. Zuidema 2014, personal communication). Surface flux estimates are used from the Woods Hole Oceanographic Institute (WHOI) objectively analyzed air–sea fluxes (OAflux), available daily on a 1° grid (Yu and Weller 2007). Ground-based radar data were obtained from the S-Pol radar at Gan Island (Feng et al. 2014). Spaceborne radar data were obtained from the Tropical Rainfall Measuring Mission (TRMM) 2A25 product (Iguchi et al. 2000). The TRMM data were processed and categorized according to the *K*-means clustering algorithm of Elsaesser et al. (2010). More details of the radar data processing are provided in section 5.

4. Estimating the Lagrangian tendency

a. *Eulerian tendency*

The first step to estimating the left-hand side of (2) is to calculate the local time tendency, otherwise known as the local Eulerian tendency. Figure 2a shows a 3-hourly time series of CWV at Gan Island (0.695°S, 73.16°E) during the DYNAMO period. This period contained three distinct MJO events with alternating dry and wet periods. The sounding dataset is a spatial interpolation among sites (Johnson and Ciesielski 2013), but at the site of the Gan sounding it mainly reflects the local direct measurement. The MIMIC satellite retrieval (Alishouse et al. 1990) suffers from saturation at high CWV values and has a hard upper limit of 64 mm, but does not seem unduly compromised in this location. The dry and transition periods show differences among the datasets, specifically around 8 October, 3 November, 10 November, 2 December, and 5 December (Fig. 2a). One thing all the datasets agree on is the existence of a distinct

Brought to you by NOAA Central Library | Unauthenticated | Downloaded 08/13/24 01:21 PM UTC

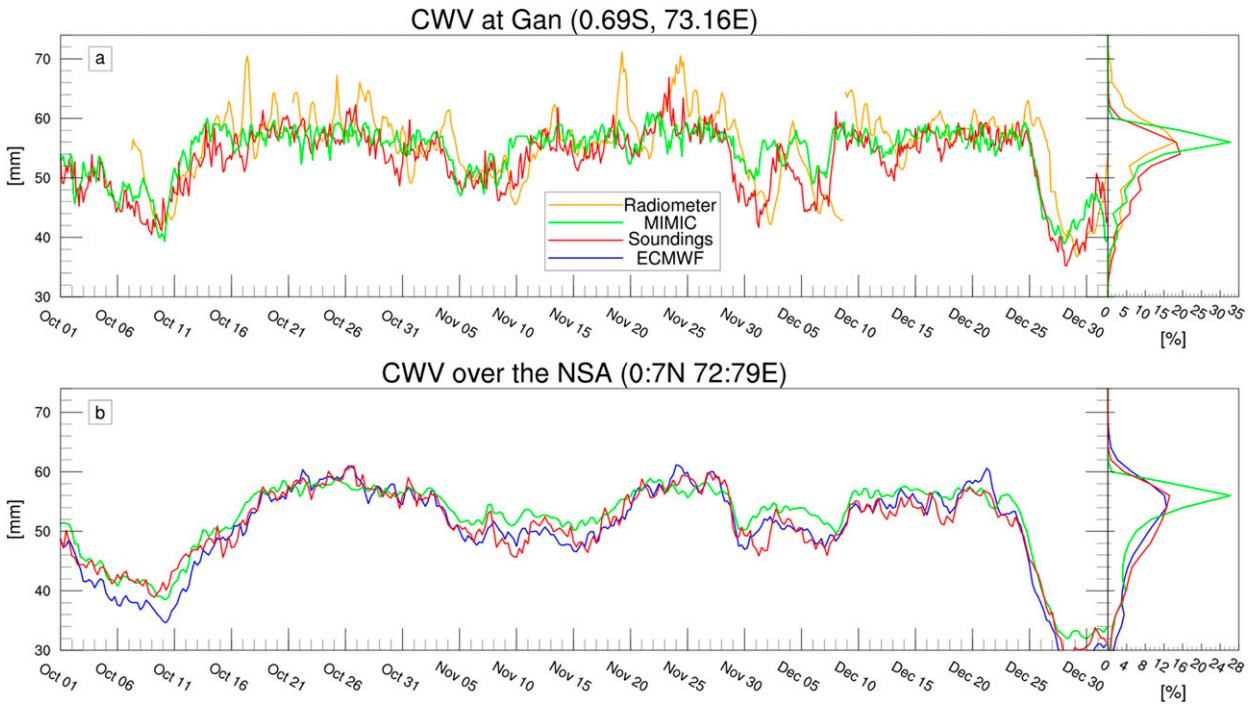

FIG. 2. Time series and frequency distribution of CWV during DYNAMO. (a) Three-hourly estimates at Gan from sounding-array data (red), a ground-based radiometer (orange), and MIMIC (green). (b) Six-hourly estimates over the NSA from sounding-array data (red), MIMIC (green), and ECMWF (blue). Note that the distributions represent all data in the domain and not the distribution of spatial averages.

mode of the frequency distribution (curves on right), corresponding to the plateau of values near 55–60 mm seen in the active periods of the three MJO cycles.

Figure 2b shows a similar CWV time series averaged over the ~500-km-sized NSA using 6-hourly data from the interpolated soundings, MIMIC, and ECMWF analysis. Averaging CWV over such a large area rounds out the time series plateaus, since the NSA is large enough to contain multiple air masses (as seen in CWV imagery below). Figure 2b also reveals inconsistencies between datasets, most notably in the dry periods. The distribution of CWV over the NSA is also smoother owing to the fact more data were used, while still exhibiting a distinct peak at 55–60 mm.

The modest differences in CWV estimates produce notable differences in the Eulerian tendency. Figure 3 illustrates this with a centered finite difference of 6-hourly data, averaged to daily and smoothed twice with a 1–2–1 filter to bring out MJO-scale variability. The largest differences of the Eulerian tendency, on the

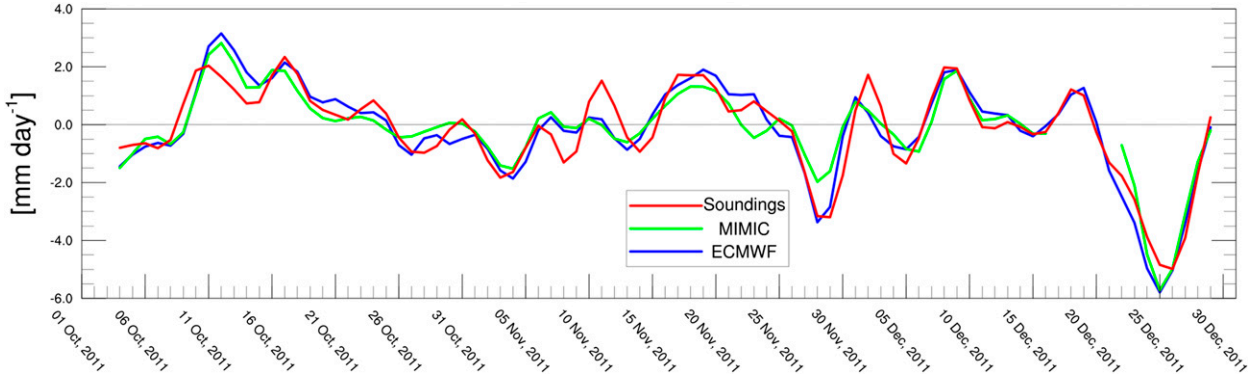

FIG. 3. Time series of the Eulerian moisture tendency estimated from the DYNAMO NSA (red), MIMIC (green), and ECMWF analysis (blue).

Brought to you by NOAA Central Library | Unauthenticated | Downloaded 08/13/24 01:21 PM UTC

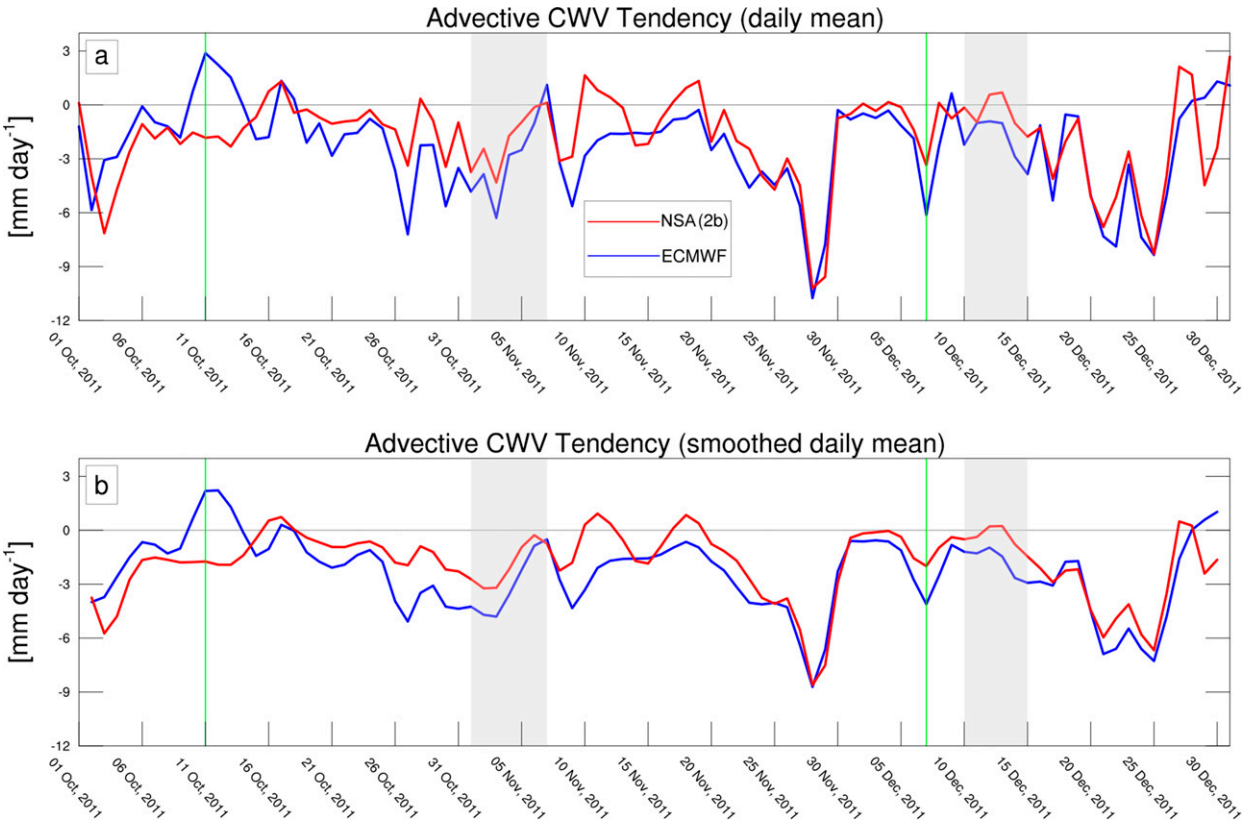

FIG. 4. (a) Time series of the advective moisture tendency estimated from the DYNAMO NSA (red) and ECMWF analysis (blue). (b) The same time series smoothed twice with a 1–2–1 filter. Thin green lines denote cases that are discussed below. Light gray shading indicates days in which the R/V *Revelle* was offsite.

order of 2–3 mm day^{-1}, occur in the dry phases of the MJO events. If these differences are not compensated by differences in horizontal advection, then they will show up as differences in the estimate of the Lagrangian tendency.

b. *Advective tendency*

The second step to estimating the left-hand side of (2) is to calculate the horizontal advective tendencies of CWV. Figure 4 shows time series of daily horizontal advective CWV tendencies, calculated from the CSU interpolated soundings and ECMWF gridded data and then averaged over the ~500-km-sized NSA. To make a fair comparison, ECMWF fields were interpolated to match the grid of the interpolated sounding dataset before calculating advection terms. There are some large differences in these two estimates of horizontal advection, which are also manifest in the 3-month average: −4.4 and −1.8 mm day^{-1} for ECMWF and sounding datasets, respectively.

Why are the differences in the advective tendency so large? Between the trusted vertical structure of the sounding data and the superior horizontal resolution of satellite data (and ECMWF's assimilation thereof), we should be able to understand the challenges. Figure 5 shows vertically resolved advective water vapor tendency for NSA averages in the two datasets. The discrepancies reside in the lower troposphere where most of the water vapor resides. The sounding data agree with the ECMWF analysis in suggesting that CWV advection has strong vertical coherence, with just 1–2 degrees of freedom (i.e., effective "layers" exhibiting quasi-independent variations) in the vertical. This is heartening, as assimilation of just a few satellite channels should suffice to capture it.

The largest discrepancy in horizontal advection occurred at 0000 UTC 11 October 2011 and can be easily understood from a snapshot of CWV and 800-hPa winds (Fig. 6). The CWV gradients are qualitatively the same as the gradient of 800 hPa q_v (not shown). Focusing on the center of the NSA (northern green polygon), we can see that the zonal gradient of water vapor has the opposite sign in ECMWF and sounding data, which results in the opposite sign of the net advective tendency when averaged over the whole area of the NSA (Figs. 4 and 5). The soundings missed a ~200-km-wide zonally oriented

Brought to you by NOAA Central Library | Unauthenticated | Downloaded 08/13/24 01:21 PM UTC

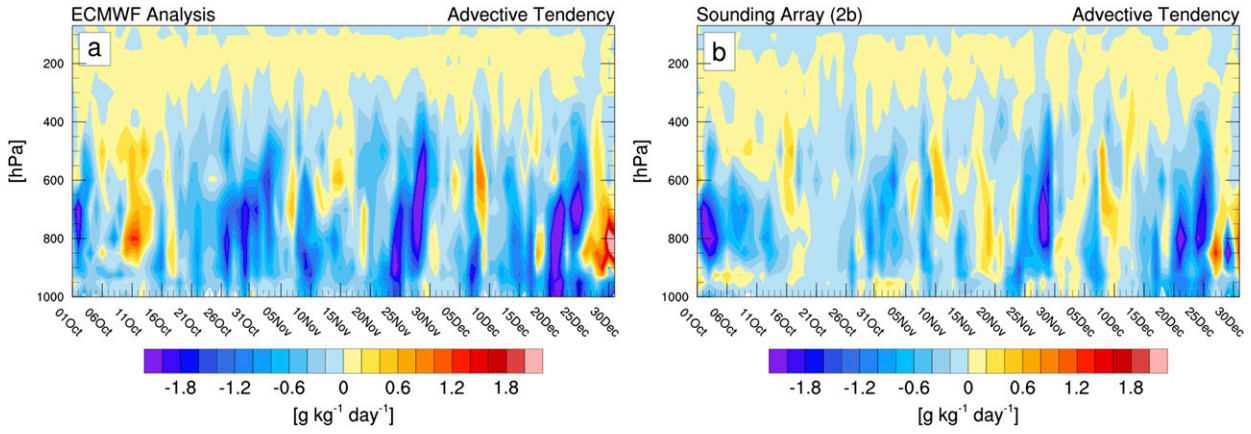

FIG. 5. Time series of the vertically resolved advective tendency of water vapor from (a) ECMWF analysis and (b) the DYNAMO NSA.

strip of relatively dry air, which lay between the two eastern vertices of the NSA. Figure 6c shows direct satellite evidence from MIMIC of this synoptic-scale dry feature, which lends confidence to its representation in ECMWF data. Hence, it seems that the low ''resolution'' (large site spacing) of the sounding array has caused an erroneous sign reversal of the advective tendency, which will ultimately have a large effect on the estimate of the LCT or apparent moisture sink at this time.

Another illustrative example can be seen at 0000 UTC 7 December 2011, during the buildup to the third MJO event observed by the NSA (Fig. 7). At this time there is northerly flow across most of the NSA, up the meridional water vapor gradient. The pattern of the wind field and CWV gradient is broadly consistent between the two datasets, but notice that the meridional gradient is much sharper in ECMWF and MIMIC data (Figs. 7b,c), which leads to a larger drying tendency that dominates

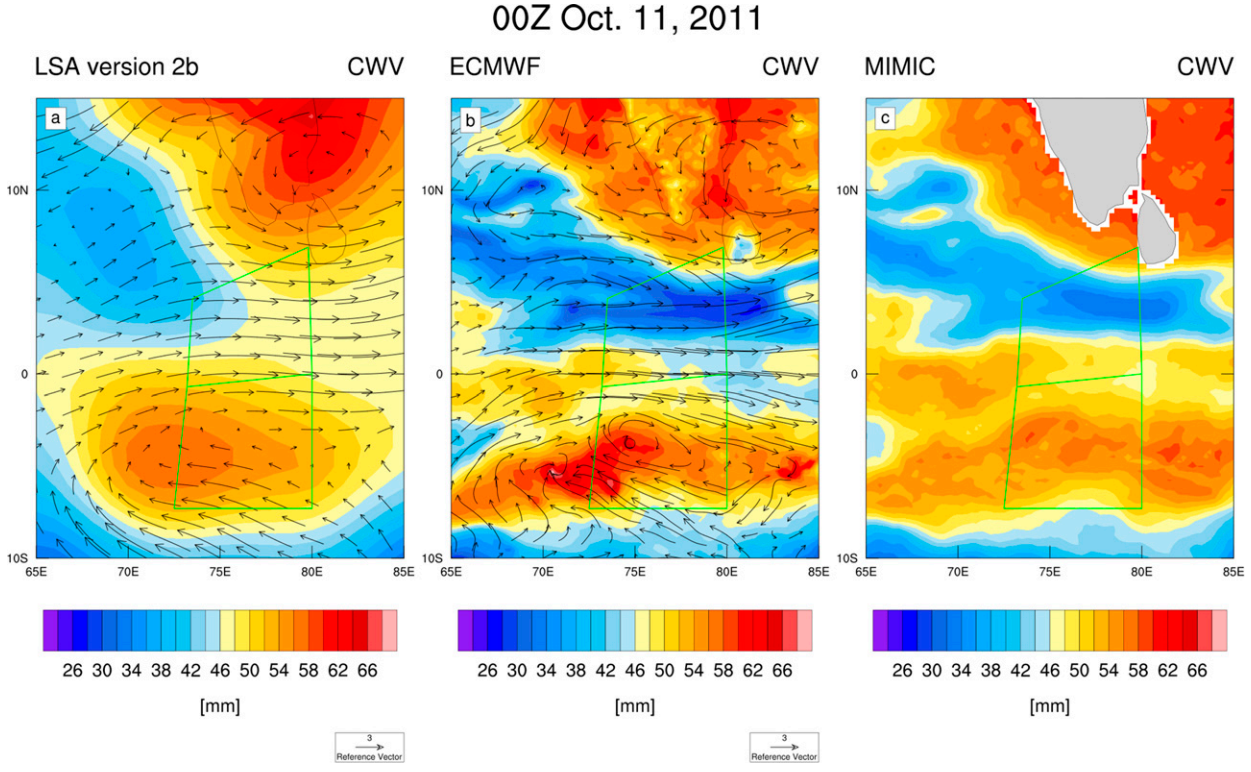

FIG. 6. Plan view of CWV and 800-hPa wind vectors from (a) DYNAMO sounding data, (b) ECMWF, and (c) MIMIC at 0000 UTC 11 Oct 2011.

Brought to you by NOAA Central Library | Unauthenticated | Downloaded 08/13/24 01:21 PM UTC

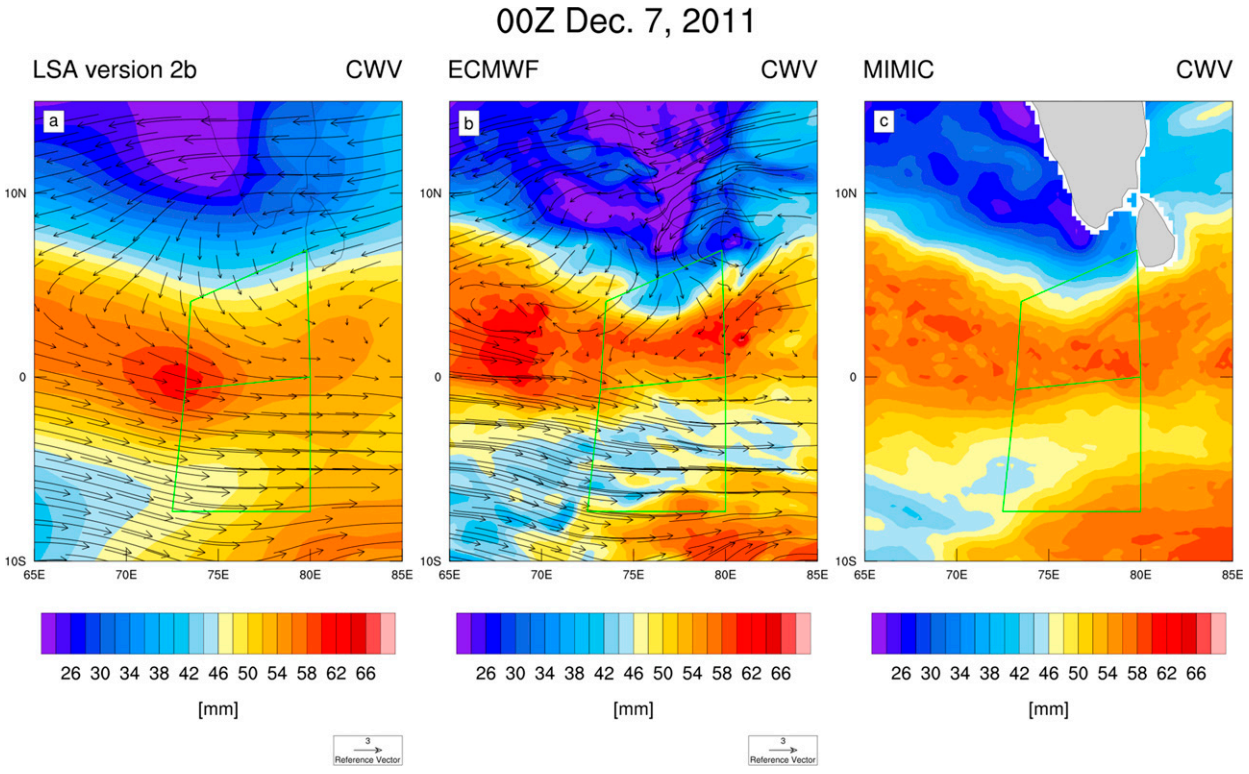

FIG. 7. As in Fig. 6, but for 0000 UTC 7 Dec 2011.

the net column advective tendency on this day (Fig. 4). Again, MIMIC data suggest that ECMWF water vapor gradients are realistic (Figs. 7b,c).

The above analysis suggests that the differences in estimates of the advective tendency represent a systematic error and reflect more of how well horizontal water vapor gradients are resolved rather than of vertical structure subtleties. Satellite data in Figs. 6 and 7 indicate that the NSA is large enough to contain more than 1 horizontal degree of freedom (based on a typical blob size in the CWV field), which leads to a systematic underestimation of advective tendencies for a sparse sounding network. We conclude that ECMWF might be the more reliable source for advective water vapor tendencies because of the superior horizontal information content. Therefore, LCT calculations below will mostly focus on the 0.25° ECMWF analyses.

c. *The Lagrangian tendency*

Figure 8 shows a smoothed time series of the daily LCT over the DYNAMO NSA, the sum of the results in Figs. 3 and 4. The LCT is almost always positive (red and blue curves), indicating a net moistening by surface evaporation minus precipitation and vertical advection. Without any smoothing the LCT is observed to occasionally be negative (not shown), which as we will see is most likely associated with periods of no convection or widespread stratiform convection.

The dashed blue line in Fig. 8 shows the result of subtracting WHOI-estimated surface evaporation from the ECWMF Lagrangian tendency (ECMWF evaporation is similar). In other words, from (2), the dashed blue line shows the residuum of wildly variable effects of the precipitation sink (shown in green) and vertical advection. The negative value of the dashed blue curve indicates that drying by precipitation outweighs the associated moistening by heating-induced upward motions. Its near-constant offset from the solid blue curve indicates that the time variations of surface evaporation do little to change the qualitative nature of the LCT time series.

The differences between ECMWF and sounding data are smallest during the westerly phase of the November and December MJO events (25–30 November and 20–25 December), suggesting that the westerly horizontal advective drying is widespread on such a large scale that it can be adequately captured by the DYNAMO sounding array.

Figure 8 indicates an in-phase relationship between CWV and LCT during the November and December MJO events. For example, during the November event, the LCT increases as CWV increases around 13–28 November. This suggests a positive feedback relationship, in which an increase in CWV is accompanied by a

Brought to you by NOAA Central Library | Unauthenticated | Downloaded 08/13/24 01:21 PM UTC

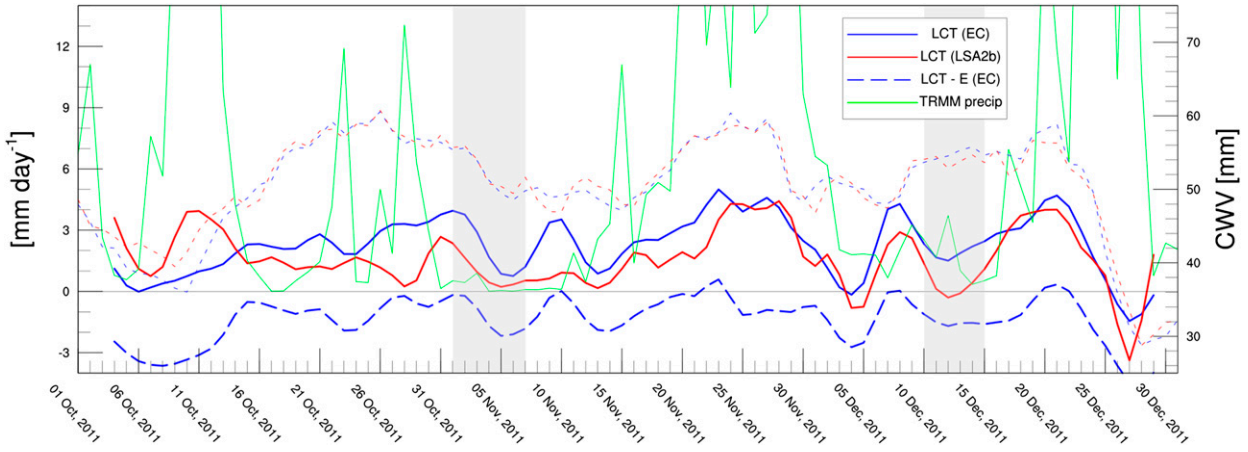

FIG. 8. Time series of the LCT (solid; left axis) and CWV (dotted; right axis) over the DYNAMO NSA for ECMWF (blue) and sounding data (red). The blue dashed line shows the ECMWF Lagrangian tendency minus WHOI surface evaporation. Light gray shading indicates days in which the R/V *Revelle* was offsite.

stronger Lagrangian moistening tendency on average. This phasing may appear somewhat inconsistent with other studies suggesting that bottom-heavy and top-heavy heating profiles play an important role in moistening and drying the column in the early and late stages of an MJO event, respectively (Lin et al. 2004; Benedict and Randall 2007; Li et al. 2009; Haertel et al. 2008; Ling and Zhang 2011; Raymond and Fuchs 2009; Fuchs et al. 2012). If convection were the primary driving force behind the MJO, we might expect the LCT and CWV to vary in quadrature, with anomalously positive LCT (i.e., moistening) in transition to the wet phase and anomalously negative LCT (i.e., drying) in transition to the dry phase. Instead, the results here show an ''in phase'' relationship between Lagrangian moistening and CWV. Still, it should be noted that this relationship is far from perfect, especially during dry periods (see also Fig. 11).

Figure 9 shows maps of the mean and standard deviation of the ECMWF LCT over the Indian Ocean overlaid with contours of the mean CWV. The highest values of the LCT occur in the ITCZ region a few degrees south of the equator (Fig. 9a), where the LCT also has the largest variability (Fig. 9b). The western sides of the Bay of Bengal and Arabian Sea also exhibit relatively high LCT variability. Interestingly, the far western equatorial Indian Ocean has a slightly negative mean Lagrangian tendency. Overall, this time-averaged map view further supports the notion that higher Lagrangian moistening generally occurs with higher CWV, consistent with a positive feedback relationship.

d. *Feedback with CWV*

A more statistical view of the relationship between CWV and LCT quantifies the notion of a positive feedback.

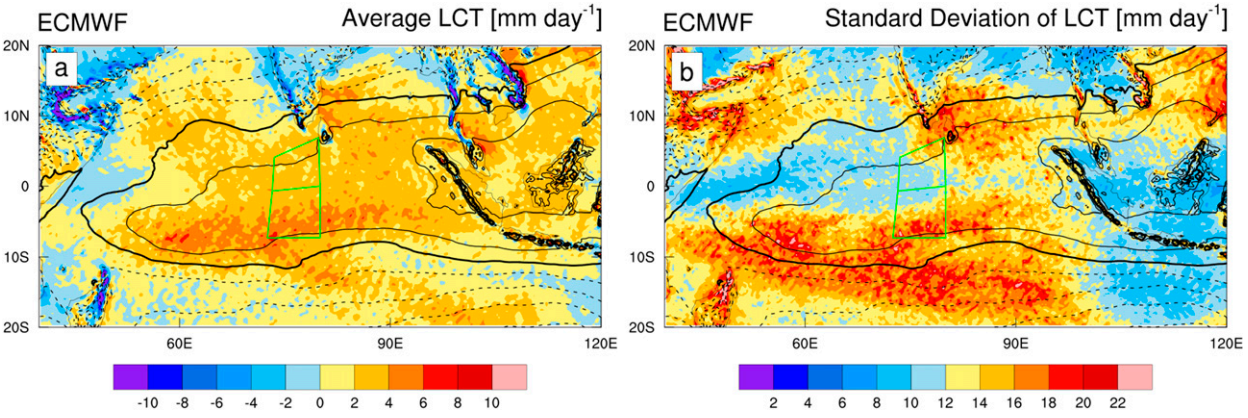

FIG. 9. (a) Map of the time-mean LCT from ECMWF data for October–December 2011 and (b) its standard deviation. Time-mean CWV is shown in overlaid contours, with contours less than 45 mm dashed.

Brought to you by NOAA Central Library | Unauthenticated | Downloaded 08/13/24 01:21 PM UTC

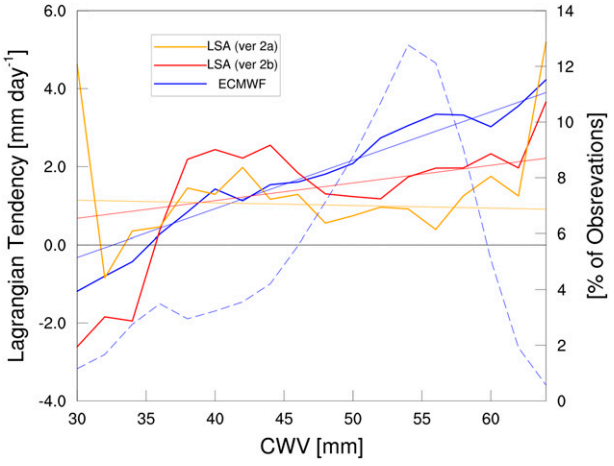

FIG. 10. Lagrangian CWV tendency binned by CWV on a 1° grid over the DYNAMO NSA (0°–7°N, 72°–79°E). Dashed curve shows the distribution of ECMWF CWV. Thin straight lines show the result of linear regression analysis.

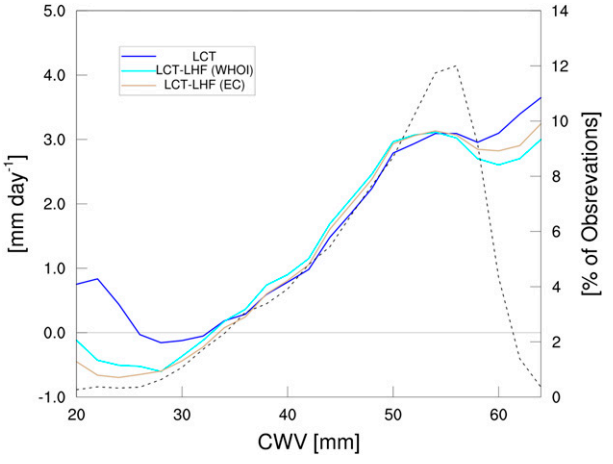

FIG. 11. ECMWF Lagrangian tendency binned by CWV over the equatorial Indian Ocean (10°S–10°N, 50°–100°E).

Figure 10 shows the LCT binned by CWV over the NSA on a 6-hourly 1° grid for ECMWF (blue) and sounding grid versions 2a and 2b (red, orange). Least squares fits are overlaid as thin lines. The results indicate a positive relationship between LCT and CWV, which is strongest in ECMWF data (whose estimates are trusted more, as discussed above). The data in Fig. 10 are limited to a small area of the Indian Ocean, so to be thorough Fig. 11 shows a similar analysis but for ECMWF data over the entire equatorial Indian Ocean (10°S–10°N, 50°–100°E) at 6-hourly and 0.25° grid scales. The positive relationship between CWV and the LCT is still evident. Figure 11 also shows the result of removing anomalous surface evaporation from both WHOI and ECWMF data (deviations from the time mean). As foreshadowed above, the effect of surface evaporation on the feedback relationship is minor, with the biggest changes occurring at the extreme ends of the distribution. The qualitative consistency between the ECMWF and WHOI data give confidence that evaporation can be removed from the LCT despite the uncertainty in observational estimates without significantly affecting the results. This is consistent with previous studies that show surface evaporation to be influenced more by wind speed, rather than the air–sea humidity difference (Riley Dellaripa and Maloney 2015). This is also consistent with the lack of a robust relationship between the LCT and horizontal advection (not shown). From the foregoing, we conclude that the positive feedback relationship is robust across the Indian Ocean and not significantly altered by surface evaporation.

The previous figures show that the Lagrangian tendency acts as a positive feedback onto the CWV when considered over a relatively large area and time period. Figure 12 further confirms that the relationship also holds for both short and long scales in space–time variability. Results for high and low temporal frequencies (blue and red lines, respectively) are isolated using a 10-day Lanczos temporal filter. Note that the difference in the position of the lines is due to the fact that filtering for high frequencies removes the time mean. Similar results are found when isolating spatial frequencies (orange and cyan lines) using 30 passes of a nine-point spatial smoothing stencil. These results are not qualitatively sensitive to cutoff frequency or filtering method (not shown). In both cases, the low-frequency data seem to exhibit a stronger positive relationship with CWV, although it is difficult to draw a strong conclusion about the significance of this given the arbitrary frequency cutoff.

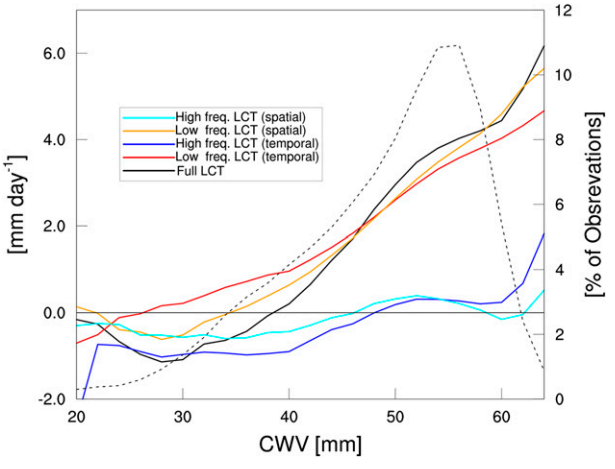

FIG. 12. ECMWF Lagrangian CWV tendency binned by CWV over the equatorial Indian Ocean (10°S–10°N, 50°–100°E) and separated into high and low frequencies, both spatially and temporally (see text).

Brought to you by NOAA Central Library | Unauthenticated | Downloaded 08/13/24 01:21 PM UTC

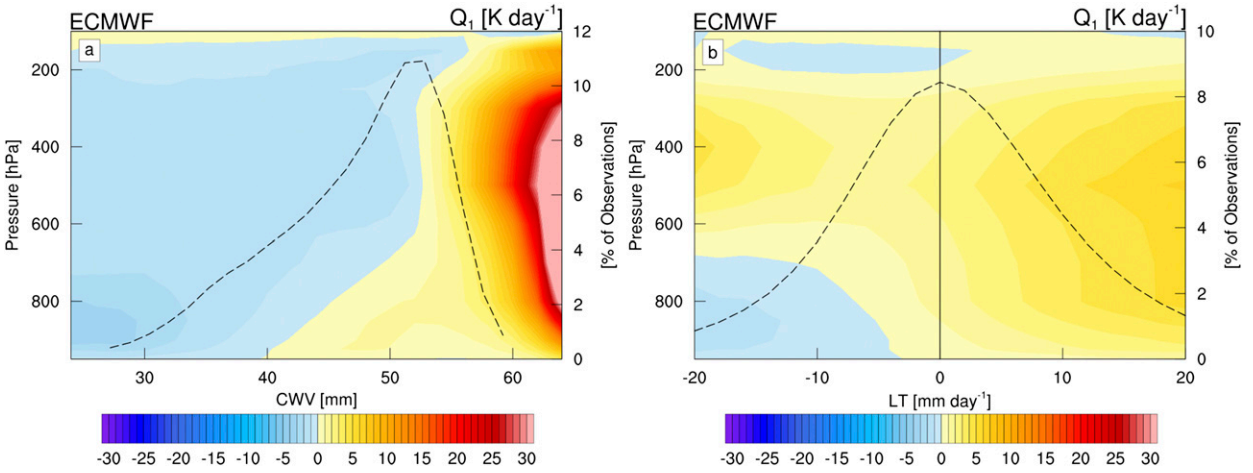

FIG. 13. The profile of Q_1 binned by (a) CWV and (b) the Lagrangian tendency over the equatorial Indian Ocean (10°S–10°N, 50°–100°E). The distribution of each variable on the abscissa is shown by the dashed line.

5. Role of convection in Lagrangian moisture dynamics

a. Heating mode analysis

Are certain cloud populations associated with Lagrangian moistening or drying of air columns in the DYNAMO-observed MJO activity? Consider an indirect measure of convection, the apparent heat source (Yanai et al. 1973), which we calculate as the nonconservation terms of the dry static energy ($s = c_pT + gz$) budget with apparent advection defined by use of the 0.25° ECMWF grid:

$$Q_1 = \partial_t s + \mathbf{v} \cdot \nabla s + \omega \partial_p s. \tag{3}$$

Figure 13 shows the profile of Q_1 binned separately by CWV and the LCT. When binned by CWV the heating profile has three basic modes: deep cooling in anomalously dry conditions, upper-level cooling above low-level heating in average conditions (~50 mm), and deep heating throughout the troposphere in anomalously wet conditions (Fig. 13a). This steep dependence of column heating on CWV agrees with the observed relationship between precipitation and CWV (Bretherton et al. 2004) and reflects the fact that convection is strongly limited by both boundary layer and tropospheric water vapor, presumably through entrainment and mixing processes affecting lifted-parcel buoyancy (Derbyshire et al. 2004; Holloway and Neelin 2009).

When Q_1 is binned by the LCT (Fig. 13b), two basic modes are seen: upper-level heating above low-level cooling (i.e., stratiform precipitation; Houze 1997) for strong Lagrangian drying and deep heating for Lagrangian moistening. Many studies have suggested that a bottom-heavy profile of heating or vertical velocity is important for the slow moistening of the column associated with the MJO (Fuchs et al. 2012; Kim et al. 2014; Benedict et al. 2014; Klingaman et al. 2015). Perhaps surprisingly, Fig. 13b does not indicate a prominent role on average for a shallow or bottom-heavy heating profile in columns undergoing a net moistening. Joint distributions of CWV and LCT will clarify the matter, but this requires the heating profile shape (i.e., convective population) to be summarized by scalar measures.

Leading modes of the Q_1 profile can be measured by two simple indices based on upper- and lower-tropospheric integrals of Q_1,

$$M_1 = Q_{\text{bottom}} + Q_{\text{top}} \quad \text{and} \tag{4}$$

$$M_2 = Q_{\text{bottom}} - Q_{\text{top}}. \tag{5}$$

We use 500 hPa as the cutoff point for the bottom and top parts of the troposphere. Figure 14 shows the profile of Q_1 regressed on the two heating mode indices M_1 and M_2. These deep and bottom-heavy heating profiles have been found to be associated with a dominance of deep cumulus and congestus convection (or stratiform precipitation with opposite sign), respectively (Johnson et al. 1999; Takayabu et al. 2010).

The joint distribution of CWV and LCT is shown in Fig. 15. Arrows describe the ''movement'' of atmospheric columns in this conceptual space. Although it is not possible to track individual columns, it is easy to see how oscillatory phenomena might trace out characteristic ''orbits'' in this space around the mean CWV.

Figure 16 shows the heating-mode indices M_1 and M_2 binned jointly by CWV and the LCT. The deep heating mode M_1 is more strongly dependent on CWV but also has a positive association with LCT. This suggests that

Brought to you by NOAA Central Library | Unauthenticated | Downloaded 08/13/24 01:21 PM UTC

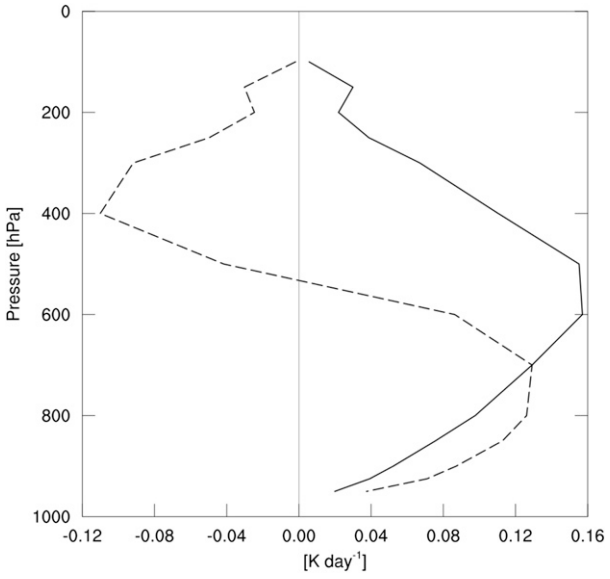

FIG. 14. The profile of Q_1 regressed against the heating-mode indices M_1 (solid) and M_2 (dashed).

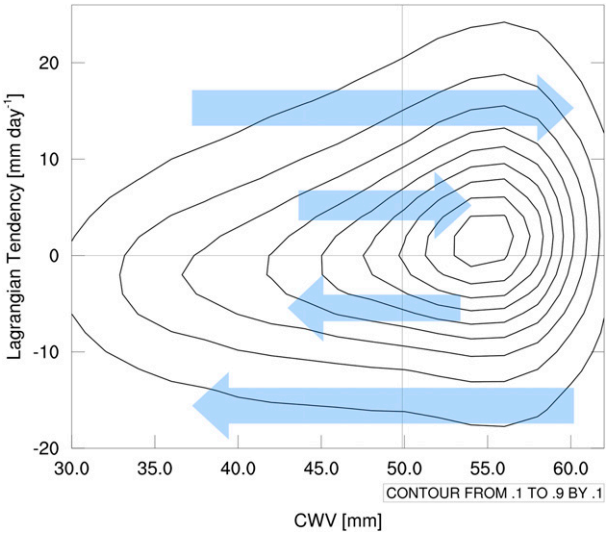

FIG. 15. Joint frequency distribution of ECMWF 6-hourly Lagrangian tendency and CWV over the equatorial Indian Ocean (10°S–10°N, 50°–100°E). Arrows indicate the qualitative trajectory of columns implied by the Lagrangian tendency. Units are percentage of the total observations. The vertical thin black line indicates the mean value of CWV.

deep convection is a key process in the positive feedback relationship suggested by the previous Figs. 10–12, at least in the ECWMF model's analysis. The bottom-heavy heating mode M_2 maximizes for positive LCT values near the mean CWV (50 mm), suggesting that bottom-heavy heating plays a significant role in columns transitioning from anomalously dry to anomalously wet conditions. There is also a notable minimum at negative LCT and large CWV (blue in Fig. 16b), corresponding to stratiform heating processes often associated with mature mesoscale convective systems (Houze 1997), which many studies have suggested may serve a crucial function in the moisture and momentum budget of the MJO (Moncrieff 2010; Benedict and Randall 2007; Khouider and Majda 2006; Seo and Wang 2010).

b. S-Pol radar observations

The results of the previous section are heavily influenced by model physics. Here we seek a comparable

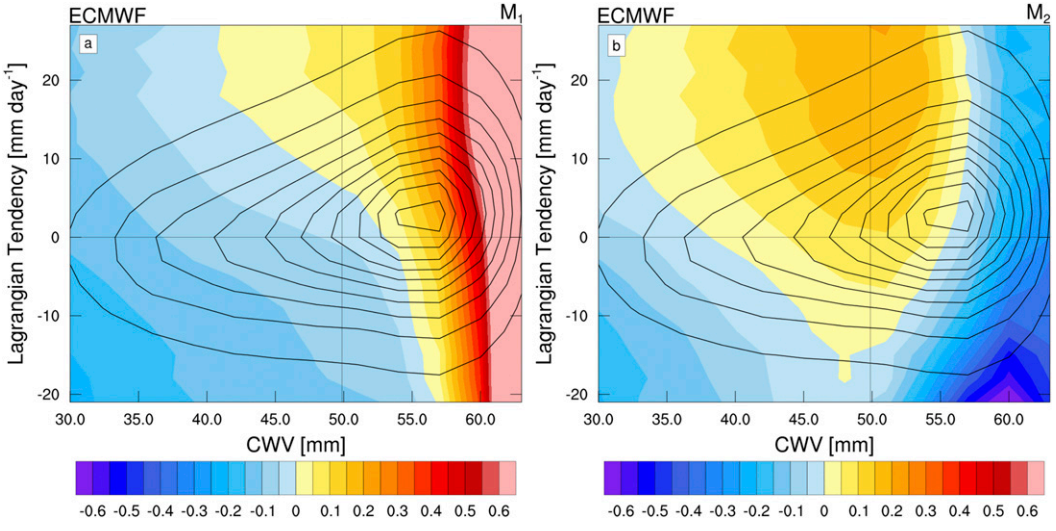

FIG. 16. Standardized heating-mode indices M_1 and M_2 binned jointly by CWV and the Lagrangian tendency from ECMWF analysis data. Data is in units of standard deviations. The joint frequency distribution is shown by the black contours. The vertical thin black line indicates the mean value of CWV.

Brought to you by NOAA Central Library | Unauthenticated | Downloaded 08/13/24 01:21 PM UTC

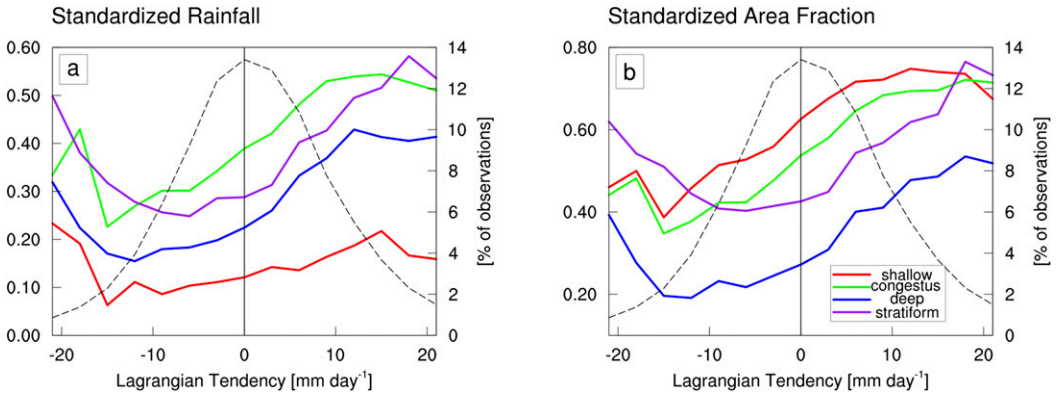

FIG. 17. Standardized (a) rainfall and (b) rain echo area fraction by convective category estimated from S-Pol radar data at Gan Island binned by the ECMWF LCT (dashed black line). Data are in units of standard deviations.

analysis of convection derived purely from direct observations, in the ECMWF analyzed CWV–LCT space. We will use two independent datasets for these direct observations: the S-Pol radar on Gan Island, which gives a lot of detail from a small spatial area, and the spaceborne radar on the TRMM satellite, which gives less detailed data over a larger area.

From the quality controlled S-Pol radar data, individual radar echo columns have been partitioned into convective, stratiform, or "other" (Feng et al. 2014). We can further break down the convective category into shallow, congestus, or deep. We define any point as congestus if it is flagged as convective and the 10-dBZ radar echo-top height is between 2.5 and 6 km. Similarly, shallow and deep convection are defined for any convective point that has a 10-dBZ echo-top height below 2.5 km or above 6 km, respectively. Note that echo features are not tracked in time, so a radar echo might be categorized as congestus at one time and deep at a later time.

We want to conditionally average radar databases on the joint distribution of ECMWF CWV and LCT estimates. Radar data are matched with the ECMWF data nearest in time, so no interpolation is used. Figure 17 shows the standardized rainfall and fractional area for each convection category of S-Pol radar data, binned by the ECMWF LCT. The fractional area is estimated during the process of regridding the radar data to match the ECMWF 0.25° grid by estimating the area covered by all rain echoes of a given convective category and then dividing by the total area of the 0.25° grid box.

Rainfall generally increases with LCT in all categories (Fig. 17), except at the tails of the LCT distribution. Shallow convective rainfall exhibits a weaker relationship with the LCT compared to the other categories.

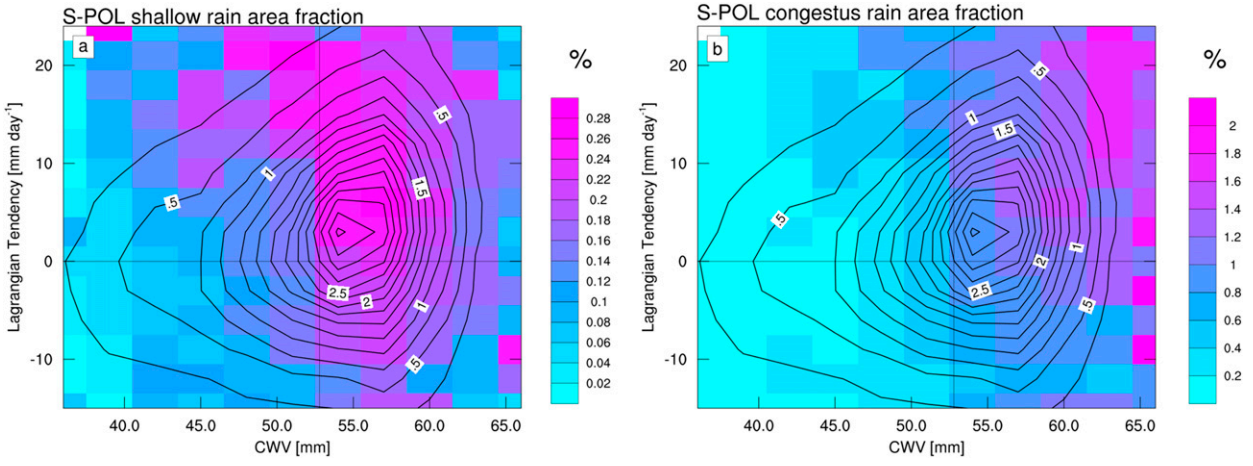

FIG. 18. S-Pol (a) shallow and (b) congestus rain area fraction binned jointly by CWV and the LCT. Contours indicate the joint distribution of CWV and the LCT. Units are percentages.

Brought to you by NOAA Central Library | Unauthenticated | Downloaded 08/13/24 01:21 PM UTC

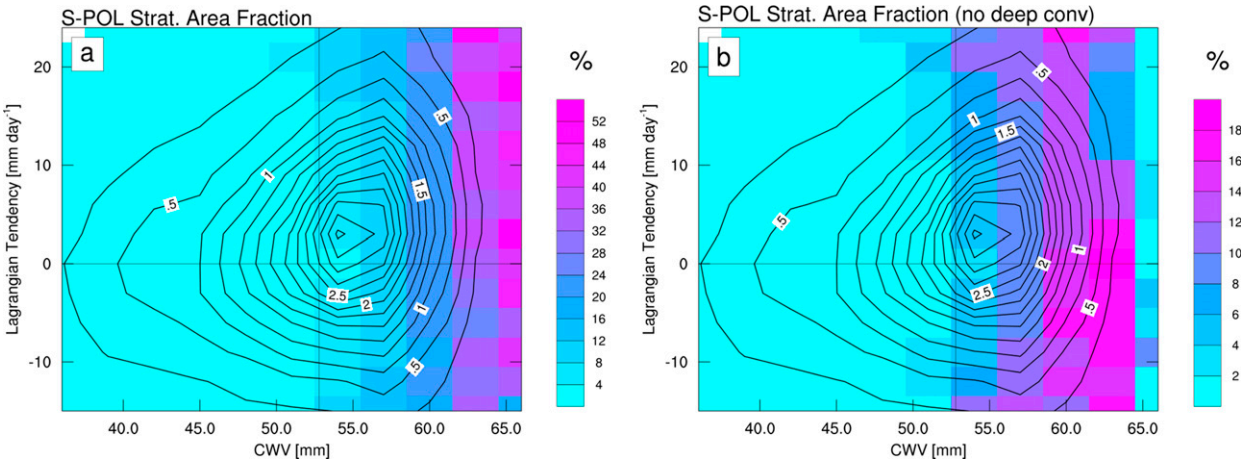

FIG. 19. S-Pol stratiform rain area fraction (a) binned jointly by CWV and the Lagrangian tendency and (b) conditionally binned when deep convection is not present (see text). Units are percentages.

The convective area fraction also exhibits a positive relationship with the LCT in all categories (Fig. 17b). The positive relationship between stratiform convection and the LCT is surprising given the results in Fig. 16b, but is likely a consequence of stratiform convection preferentially occurring in the presence of deep convection, which shows a strong positive relationship with LCT. The results in Fig. 17 were found to be similar when using daily averages or SPOL-domain-averaged data (~3° scale; not shown). We are most interested in characterizing the cloud population, rather than how much rain is produced, and thus the following analysis will focus on the convective area fraction.

Figure 18 shows the S-Pol fractional area data jointly binned by CWV and LCT. S-Pol shallow and congestus fractional area are greatest in positive LCT conditions, consistent with conventional wisdom that an abundance of these cloud types is associated with moistening. The shallow convective fractional area pattern looks similar to the pattern of the second baroclinic heating mode in Fig. 16b, while congestus area fraction peaks at the higher CWV values, which may be because we are inadvertently sampling deep convective clouds early in their development.

Similar analysis of deep convective area fraction shows a strong dependence on CWV, which overwhelms any noticeable dependence on LCT (not shown). Figure 19a shows the stratiform rain area fraction binned jointly by CWV and LCT, and again its strong dependence on CWV spoils any resemblance to Fig. 16b.

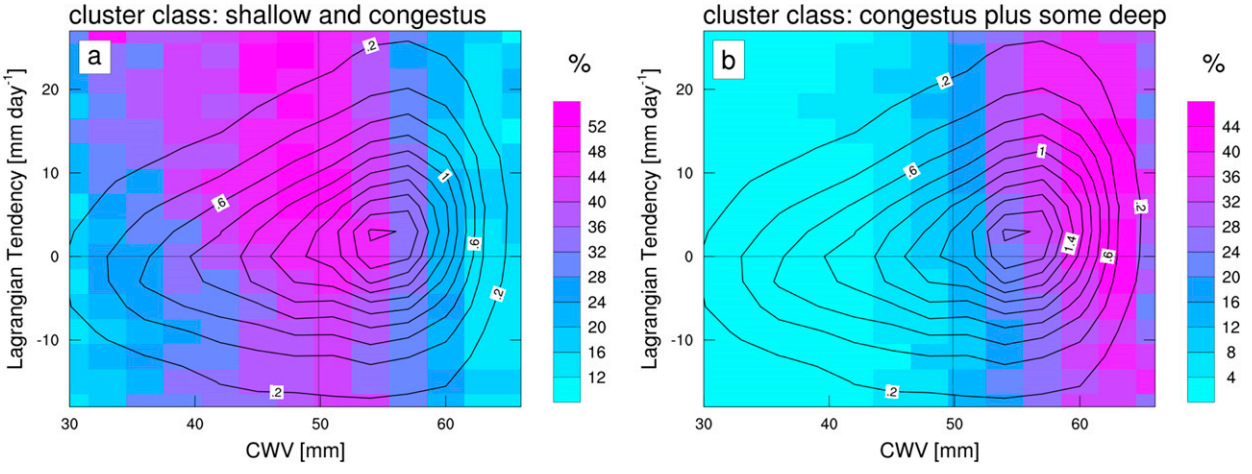

FIG. 20. Percentage frequency of occurrence of TRMM (a) shallow and congestus and (b) congestus and deep convection rain scenes identified by the *K*-means clustering algorithm (see text) binned jointly by LCT and CWV in shading. Data were used from the equatorial Indian Ocean (10°S–10°N, 50°–100°E). Contours indicate the joint distribution of CWV and the LCT.

Brought to you by NOAA Central Library | Unauthenticated | Downloaded 08/13/24 01:21 PM UTC

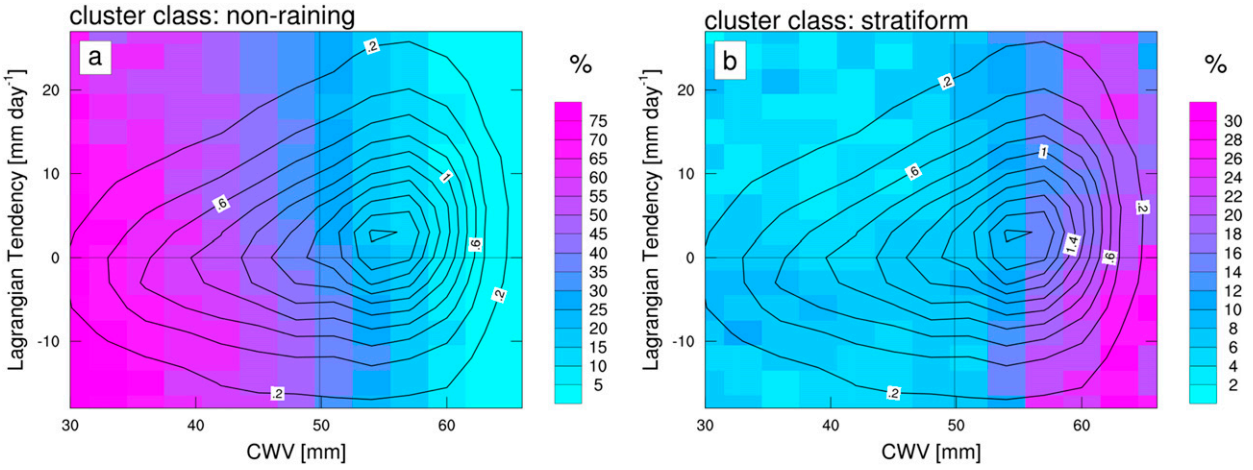

FIG. 21. As in Fig. 20, but for (a) nonraining and (b) stratiform precipitation scene.

However, when we repeat this analysis and only consider times when the area fraction of deep convection is less than 5% (Fig. 19b), the pattern peaks at high CWV and negative LCT like in Fig. 16b. In summary, S-Pol radar data are consistent with our expectations in that stratiform precipitation is associated with Lagrangian drying, but this signal is complicated by its coexistence with deep convection.

c. *TRMM Precipitation Radar observations*

To increase sample size from the ground-based radar results of the previous section, spaceborne precipitation radar (PR) rain-rate and echo-top-height (ETH) data from the Tropical Rainfall Measuring Mission (TRMM) during the DYNAMO period are shown in Figs. 20 and 21. Our approach to processing the TRMM data is based on the study of Elsaesser et al. (2010), in which a *K*-means clustering algorithm is used to classify TRMM precipitation scenes. The level 2 TRMM PR data are on a 5-km grid, but clusters (scene types) are estimated on a 1° grid.

The *K*-means clustering algorithm uses five TRMM PR variables:

1) the number of convective pixels with an ETH less than 5 km,
2) the number of convective pixels with an ETH between 5 and 9 km,
3) the number of convective pixels with an ETH greater than 9 km,
4) the average convective rain rate over the grid cell, and
5) the average rain rate over the grid cell.

Note that the heights of the convective classes in this section do not match those used for the ground-based radar data in the previous section because the TRMM PR is less sensitive with 17-dBZ instead of 10-dBZ detection cutoff. It is also important to recognize that the determination of convective or stratiform rain is complicated by several factors that can lead to convective clouds to be misclassified as stratiform (Schumacher and Houze 2003; Funk et al. 2013). The *K*-means algorithm produces three precipitation clusters, plus two additional cluster types when the scene has either no rain or mostly stratiform rain. The resulting five cluster classes from the algorithm are interpreted as follows:

1) shallow and congestus convection,
2) congestus plus some deep convection,
3) deep convection with some stratiform,
4) widespread stratiform, and
5) nonraining.

Figure 20 shows the percentage frequency of occurrence of shallow and congestus cloud categories using all available data from the equatorial Indian Ocean (10°S–10°N, 50°–100°E) during DYNAMO (1 October–15 December 2011). The frequency of occurrence is calculated in each joint histogram bin by dividing the number of points of a given convective category by the total number of data points in the bin. Comparing Figs. 20 and 18, we can see that the TRMM data match the characteristic pattern from S-Pol, with both shallow and congestus cloud scenes occurring more often with a positive Lagrangian tendency. TRMM congestus scenes tend to occur in wetter environments with a positive LCT. The deep convective cluster is found to have a strong dependence on CWV and no noticeable dependence on LCT, which is also consistent with S-Pol results (not shown).

Brought to you by NOAA Central Library | Unauthenticated | Downloaded 08/13/24 01:21 PM UTC

Nonraining and stratiform TRMM scenes are shown in Fig. 21. Both clusters show a mild propensity to occur with negative LCT. The stratiform cluster shows a clear preference for negative LCT, resembling Fig. 19b, since the cluster analysis required no deep convection to be present (on 1° scale) in order to classify the scene as stratiform. The tendency for nonraining scenes to be associated negative LCT is consistent with the notion that a column dominated by radiative cooling should exhibit widespread subsidence and a net divergence of column water vapor (see also Fig. 16a).

The S-Pol and TRMM data represent two independent indications that shallow and congestus convection preferentially occur with Lagrangian moistening of an air column. Similarly, both radar datasets indicate that scenes with widespread stratiform precipitation in the absence of deep convection, as well as nonraining scenes, tend to be associated with Lagrangian drying, as diagnosed from ECMWF analysis CWV and LCT estimates.

6. Summary and discussion

a. Summary

This study presents a novel approach to studying column water vapor dynamics, which are thought to be crucial to the MJO, and seeks to connect large-scale water vapor patterns to localized cloud and precipitation data from a field campaign. A Lagrangian column water vapor (CWV) budget framework usefully combines condensation and vertical advective moisture tendencies, which are intimately coupled and impossible to estimate separately to an accuracy useful for MJO evolution process studies. The Lagrangian CWV tendency (LCT) is our key quantity, estimated on the budget's left-hand side as the residual of the Eulerian and horizontal advective CWV tendencies. These terms are reasonably well estimated in ECMWF analyses, which assimilate abundant and accurate marine microwave satellite data. The moisture budget terms are not well estimated in interpolated sounding-array data because CWV features are of smaller scale than field-campaign site spacing. Ultimately, the relevance of this horizontally Lagrangian view hinges on the longevity and coherence of such CWV features, as indicated by satellite animations (see also Fig. 1).

The LCT increases with increasing CWV, suggesting a positive feedback relationship. Further decomposition of slow and fast time scales, and long and short spatial scales, show that the positive relationship between the LCT and CWV is robust, from time series to spatial structure to a wide range of space–time variability. The distinct moist mode in the CWV probability distribution (Fig. 2) is a reflection of these conditional dynamics of LCT, although additional processes such as horizontal convergence and diffusion must be active in shaping the upper end of the distribution.

Analysis of convective heating profiles showed the expected result that bottom-heavy heating profiles tend to be associated with Lagrangian moistening, and top-heavy profiles tend to be associated with Lagrangian drying, consistent with ideas of negative and positive gross moist stability (Raymond et al. 2009). Ground-based S-Pol radar data from Gan Island show that the fractional area of shallow and congestus convection tends to be largest when LCT is positive. Similarly, stratiform precipitation in S-Pol data was found to be associated with Lagrangian drying, but only after the data had been screened for times when deep convection was not abundant. Analysis of categorized scenes in TRMM spaceborne radar data also show that shallow and congestus convection preferentially occur with Lagrangian moistening, whereas stratiform rain and nonraining scenes are associated with Lagrangian drying.

b. Discussion

The Lagrangian approach used here has some distinct advantages compared to a more traditional Eulerian framework. Many studies that have analyzed thermodynamic budgets in the tropics have chosen to consider variations in all terms separately and explore further decompositions (e.g., Maloney 2009; Hannah and Maloney 2011; Kiranmayi and Maloney 2011; Cai et al. 2013; Hannah and Maloney 2014; Masunaga and L'Ecuyer 2014). This approach has yielded many insights into the MJO as well as the general nature of moist convection in the tropics. However, the Eulerian approach leaves some ambiguity in determining the importance of the advective tendency to moisture variability in the presence of an anomalously moist air mass that is moving, such as the MJO envelope. The Lagrangian approach sidesteps this uncertainty by combining the advective and local Eulerian tendencies so local moisture variability caused by a moving air mass will not affect the Lagrangian tendency. The other advantage of a Lagrangian approach is that we avoid the artificial separation of moisture convergence and precipitation. In either case, we still do not have a way to know how much of the moisture convergence is driven by convection and how much is driven by large-scale motions associated with waves or the general circulation. Overall, the Lagrangian framework is a promising tool for probing the nature of tropical convection.

Our choice of CWV over a conserved moist-thermodynamic quantity, such as moist static energy

Brought to you by NOAA Central Library | Unauthenticated | Downloaded 08/13/24 01:21 PM UTC

(MSE) or moist entropy, is driven by observational and diagnostic considerations. The hardest quantities to observe or estimate are precipitation and vertical velocity w, owing to their extremely spotty and skewed characteristics. The present approach is one way to sidestep these observational challenges. It arguably has advantages over MSE, which eliminates precipitation, but leaves w in a vertical advection term that lingers in the form of the nonuniversal, scale- and phenomenon-dependent, and debatably misnamed quantity gross moist stablity (GMS). Redoing some of the analysis presented here with the MSE budget produces very similar results (not shown), as it must since column temperature varies little in the domain of our study. In our approach, cloud–radiative effects are implicit in the slight imbalance between vertical moisture advection and phase change, while in the MSE budget they are front and center. Studies focused on different processes must therefore choose whichever quantity is appropriate.

It would be very convenient if the vertical structure of the diabatic heating profile (i.e., M_1 and M_2) or a characterization of the cloud population was sufficient to determine the sign of the LCT. Figures 16b and 18–21 suggest that this is not possible because none of the heating modes or cloud types is confined to one sign of the LCT. This also holds when variations of surface evaporation are considered (not shown). In other words, there is no threshold of shallow convective fraction or stratiform fraction that we can say will guarantee Lagrangian moistening or drying, respectively. Instead, we need to have a more comprehensive view of the impacts of radiatively driven subsidence (e.g., Chikira 2014), surface fluxes, and large-scale convergence not associated with convection to really understand the role convection plays in the large-scale moisture variability of the tropics.

The Lagrangian framework for studying moisture dynamics presented here would make a useful metric for evaluating large-scale models. To begin with, the sharp mode in the CWV (representing shifting, advecting plateau areas of high values in CWV maps and animations) should be reproduced. This will depend on feedbacks between parameterized physics and dynamics, so it already cannot be taken for granted. The shape of the LCT versus CWV (i.e., Fig. 11) and the relationship between the diabatic heating profile and the LCT (i.e., Fig. 16) can also be scrutinized to assess the overall moisture dynamics of a model.

Having established that analyzed data are adequate (i.e., that special field-campaign data are not essential to seeing some of the signals identified here), a more extensive characterization of CWV and its LCT should be undertaken, since our analysis only considers a specific season and region of the tropics. Clarity might also be optimized by refining the analysis to the scales at which CWV exhibits the most coherent and long-lived features. Here the 0.25° data from ECWMF appeared a bit noisy with untrusted smallest-scale features (Figs. 6 and 7) potentially diluting the statistics. Perhaps assimilated winds combined with more direct satellite-derived CWV fields, as embodied in the MIMIC product, could be a useful refinement.

A noteworthy caveat of the radar analysis in this work is that the data includes the diurnal cycle, which slightly changes the characteristic shape of the joint distribution. Daily mean data may have been more appropriate for interpreting our results in the context of the MJO, but attempts to utilize daily means clearly showed that there was insufficient data to make robust conclusions. TRMM offers much more data, but since we were using the level 2 orbital data, it is not possible to obtain sufficient samples for a daily mean at any single location. Composite analysis of TRMM data over a much longer period may remedy this issue. Also, further analysis of ground-based radar sites with long records may provide enough data to consider daily mean analysis.

Our methods here were heavily reliant on analysis data (whose strengths include satellite inputs), but a less model-influenced estimate of the LCT may be possible with denser sounding networks or satellite data directly. Advancements in unmanned aerial vehicles may make denser sounding networks over the ocean a reality in the near future, which would also potentially lower the overall cost of gathering field observations. Tracking CWV features between satellite passes could give a direct estimate of Lagrangian temporal changes without the explicit multistep bookkeeping of section 4 using analyses of wind profiles, moisture profiles, their product, and its integral. Further work in that direction is underway, by deconstructing the Wimmers and Velden (2011) data product that motivated this study, and will be reported elsewhere.

Acknowledgments. The authors thank Dr. Paquita Zuidema for providing the Gan radiometer data and Dr. Matt Janiga for his assistance obtaining the S-Pol radar data used in this study. The authors appreciate feedback from Adam Sobel and two anonymous reviewers, as their comments greatly helped to improve this manuscript. This work was supported by Award NA13OAR4310156 from NOAA, U.S. Department of Commerce. The statements, findings, conclusions, and recommendations do not necessarily reflect the views of NOAA or the Department of Commerce. Brian Mapes also acknowledges support from NASA Grants

Brought to you by NOAA Central Library | Unauthenticated | Downloaded 08/13/24 01:21 PM UTC

NNX13AQ50G and NNX15AD11G, DOE Award Number DE-SC0006806, and ONR Grant N000141310704.

REFERENCES

Adames, Á. F., and D. Kim, 2016: The MJO as a dispersive, convectively coupled moisture wave: Theory and observations. *J. Atmos. Sci.*, **73**, 913–941, doi:10.1175/JAS-D-15-0170.1.

Adams, D. K., and Coauthors, 2015: The Amazon Dense GNSS Meteorological Network: A new approach for examining water vapor and deep convection interactions in the tropics. *Bull. Amer. Meteor. Soc.*, **96**, 2151–2165, doi:10.1175/BAMS-D-13-00171.1.

Alishouse, J. C., S. A. Snyder, J. Vongsathorn, and R. R. Ferraro, 1990: Determination of oceanic total precipitable water from the SSM/I. *IEEE Trans. Geosci. Remote Sens.*, **28**, 811–816, doi:10.1109/36.58967.

Andersen, J. A., and Z. Kuang, 2012: Moist static energy budget of MJO-like disturbances in the atmosphere of a zonally symmetric aquaplanet. *J. Climate*, **25**, 2782–2804, doi:10.1175/JCLI-D-11-00168.1.

Benedict, J. J., and D. Randall, 2007: Observed characteristics of the MJO relative to maximum rainfall. *J. Atmos. Sci.*, **64**, 2332–2354, doi:10.1175/JAS3968.1.

——, E. D. Maloney, A. H. Sobel, and D. M. W. Frierson, 2014: Gross moist stability and MJO simulation skill in three full-physics GCMs. *J. Atmos. Sci.*, **71**, 3327–3349, doi:10.1175/JAS-D-13-0240.1.

Bretherton, C., M. Peters, and L. Back, 2004: Relationships between water vapor path and precipitation over the tropical oceans. *J. Climate*, **17**, 1517–1528, doi:10.1175/1520-0442(2004)017<1517:RBWVPA>2.0.CO;2.

Cai, Q., G. J. Zhang, and T. Zhou, 2013: Impacts of shallow convection on MJO simulation: A moist static energy and moisture budget analysis. *J. Climate*, **26**, 2417–2431, doi:10.1175/JCLI-D-12-00127.1.

Charney, J., 1963: A note of large-scale motions in the tropics. *J. Atmos. Sci.*, **20**, 607–609, doi:10.1175/1520-0469(1963)020<0607:ANOLSM>2.0.CO;2.

Chikira, M., 2014: Eastward-propagating intraseasonal oscillation represented by Chikira–Sugiyama cumulus parameterization. Part II: Understanding moisture variation under weak temperature gradient balance. *J. Atmos. Sci.*, **71**, 615–639, doi:10.1175/JAS-D-13-038.1.

Ciesielski, P. E., and Coauthors, 2014: Quality-controlled upper-air sounding dataset for DYNAMO/CINDY/AMIE: Development and corrections. *J. Atmos. Oceanic Technol.*, **31**, 741–764, doi:10.1175/JTECH-D-13-00165.1.

Derbyshire, S. H., I. Beau, P. Bechtold, J.-Y. Grandpeix, J.-M. Pirou, J.-L. Redelsperger, and P. M. M. Soares, 2004: Sensitivity of moist convection to environmental humidity. *Quart. J. Roy. Meteor. Soc.*, **130**, 3055–3079, doi:10.1256/qj.03.130.

Elsaesser, G. S., C. D. Kummerow, T. S. Lecuyer, Y. N. Takayabu, and S. Shige, 2010: Observed self-similarity of precipitation regimes over the tropical oceans. *J. Climate*, **23**, 2686–2698, doi:10.1175/2010JCLI3330.1.

Feng, Z., S. A. McFarlane, C. Schumacher, S. Ellis, J. Comstock, and N. Bharadwaj, 2014: Constructing a merged cloud–precipitation radar dataset for tropical convective clouds during the DYNAMO/AMIE experiment at Addu Atoll. *J. Atmos. Oceanic Technol.*, **31**, 1021–1042, doi:10.1175/JTECH-D-13-00132.1.

Fuchs, Ž., S. Gjorgjievska, and D. J. Raymond, 2012: Effects of varying the shape of the convective heating profile on convectively coupled gravity waves and moisture modes. *J. Atmos. Sci.*, **69**, 2505–2519, doi:10.1175/JAS-D-11-0308.1.

Funk, A., C. Schumacher, and J. Awaka, 2013: Analysis of rain classifications over the tropics by version 7 of the TRMM PR 2A23 algorithm. *J. Meteor. Soc. Japan*, **91**, 257–271, doi:10.2151/jmsj.2013-302.

Haertel, P. T., G. N. Kiladis, A. Denno, and T. M. Rickenbach, 2008: Vertical-mode decompositions of 2-day waves and the Madden–Julian oscillation. *J. Atmos. Sci.*, **65**, 813–833, doi:10.1175/2007JAS2314.1.

Hannah, W. M., and E. D. Maloney, 2011: The role of moisture–convection feedbacks in simulating the Madden–Julian oscillation. *J. Climate*, **24**, 2754–2770, doi:10.1175/2011JCLI3803.1.

——, and ——, 2014: The moist static energy budget in NCAR CAM5 hindcasts during DYNAMO. *J. Adv. Model. Earth Syst.*, **6**, 420–440, doi:10.1002/2013MS000272.

Holloway, C. E., and J. D. Neelin, 2009: Moisture vertical structure, column water vapor, and tropical deep convection. *J. Atmos. Sci.*, **66**, 1665–1683, doi:10.1175/2008JAS2806.1.

Houze, R. A., 1997: Stratiform precipitation in regions of convection: A meteorological paradox? *Bull. Amer. Meteor. Soc.*, **78**, 2179–2196, doi:10.1175/1520-0477(1997)078<2179:SPIROC>2.0.CO;2.

Iguchi, T., T. Kozu, R. Meneghini, J. Awaka, and K. Okamoto, 2000: Rain-profiling algorithm for the TRMM Precipitation Radar. *J. Appl. Meteor.*, **39**, 2038–2052, doi:10.1175/1520-0450(2001)040<2038:RPAFTT>2.0.CO;2.

Johnson, R. H., and P. E. Ciesielski, 2013: Structure and properties of Madden–Julian oscillations deduced from DYNAMO sounding arrays. *J. Atmos. Sci.*, **70**, 3157–3179, doi:10.1175/JAS-D-13-065.1.

——, T. M. Rickenbach, S. A. Rutledge, P. E. Ciesielski, and W. H. Schubert, 1999: Trimodal characteristics of tropical convection. *J. Climate*, **12**, 2397–2418, doi:10.1175/1520-0442(1999)012<2397:TCOTC>2.0.CO;2.

Khouider, B., and A. Majda, 2006: A simple multicloud parameterization for convectively coupled tropical waves. Part I: Linear analysis. *J. Atmos. Sci.*, **63**, 1308–1323, doi:10.1175/JAS3677.1.

Kidd, C., and G. Huffman, 2011: Global precipitation measurement. *Meteor. Appl.*, **18**, 334–353, doi:10.1002/met.284.

Kiladis, G. N., M. C. Wheeler, P. T. Haertel, K. H. Straub, and P. E. Roundy, 2009: Convectively coupled equatorial waves. *Rev. Geophys.*, **47**, 1–42, doi:10.1029/2008RG000266.

Kim, D., and Coauthors, 2014: Process-oriented MJO simulation diagnostic: Moisture sensitivity of simulated convection. *J. Climate*, **27**, 5379–5395, doi:10.1175/JCLI-D-13-00497.1.

Kiranmayi, L., and E. D. Maloney, 2011: Intraseasonal moist static energy budget in reanalysis data. *J. Geophys. Res.*, **116**, D21117, doi:10.1029/2011JD016031.

Klingaman, N. P., and Coauthors, 2015: Vertical structure and diabatic processes of the Madden–Julian oscillation: Linking hindcast fidelity to simulated diabatic heating and moistening. *J. Geophys. Res. Atmos.*, **120**, 4690–4717, doi:10.1002/2014JD022374.

Krajewski, W. F., and J. A. Smith, 2002: Radar hydrology: Rainfall estimation. *Adv. Water Resour.*, **25**, 1387–1394, doi:10.1016/S0309-1708(02)00062-3.

Brought to you by NOAA Central Library | Unauthenticated | Downloaded 08/13/24 01:21 PM UTC

Kuang, Z., 2008: A moisture–stratiform instability for convectively coupled waves. *J. Atmos. Sci.*, **65**, 834–854, doi:10.1175/2007JAS2444.1.

Li, C., X. Jia, J. Ling, W. Zhou, and C. Zhang, 2009: Sensitivity of MJO simulations to diabatic heating profiles. *Climate Dyn.*, **32**, 167–187, doi:10.1007/s00382-008-0455-x.

Lin, J., B. Mapes, M. Zhang, and M. Newman, 2004: Stratiform precipitation, vertical heating profiles, and the Madden–Julian oscillation. *J. Atmos. Sci.*, **61**, 296–309, doi:10.1175/1520-0469(2004)061<0296:SPVHPA>2.0.CO;2.

Ling, J., and C. Zhang, 2011: Structural evolution in heating profiles of the MJO in global reanalyses and TRMM retrievals. *J. Climate*, **24**, 825–842, doi:10.1175/2010JCLI3826.1.

Madden, R. A., and P. R. Julian, 1972: Description of global-scale circulation cells in the tropics with a 40–50 day period. *J. Atmos. Sci.*, **29**, 1109–1123, doi:10.1175/1520-0469(1972)029<1109:DOGSCC>2.0.CO;2.

Maloney, E. D., 2009: The moist static energy budget of a composite tropical intraseasonal oscillation in a climate model. *J. Climate*, **22**, 711–729, doi:10.1175/2008JCLI2542.1.

Mapes, B. E., 2000: Convective inhibition, subgrid-scale triggering energy, and stratiform instability in a toy tropical wave model. *J. Atmos. Sci.*, **57**, 1515–1535, doi:10.1175/1520-0469(2000)057<1515:CISSTE>2.0.CO;2.

——, S. Tulich, J. Lin, and P. Zuidema, 2006: The mesoscale convection life cycle: Building block or prototype for large-scale tropical waves? *Dyn. Atmos. Oceans*, **42**, 3–29, doi:10.1016/j.dynatmoce.2006.03.003.

Masunaga, H., and T. S. L'Ecuyer, 2014: A mechanism of tropical convection inferred from observed variability in the moist static energy budget. *J. Atmos. Sci.*, **71**, 3747–3766, doi:10.1175/JAS-D-14-0015.1.

Moncrieff, M. W., 2010: The multiscale organization of moist convection and the intersection of weather and climate. *Climate Dynamics: Why Does Climate Vary?*, *Geophys. Monogr.*, Vol. 189, Amer. Geophys. Union, 3–26.

Neelin, J. D., and I. M. Held, 1987: Modeling tropical convergence based on the moist static energy budget. *Mon. Wea. Rev.*, **115**, 3–12, doi:10.1175/1520-0493(1987)115<0003:MTCBOT>2.0.CO;2.

Raymond, D. J., 2001: A new model of the Madden–Julian oscillation. *J. Atmos. Sci.*, **58**, 2807–2819, doi:10.1175/1520-0469(2001)058<2807:ANMOTM>2.0.CO;2.

——, and Ž. Fuchs, 2009: Moisture modes and the Madden–Julian oscillation. *J. Climate*, **22**, 3031–3046, doi:10.1175/2008JCLI2739.1.

——, S. L. Sessions, A. H. Sobel, and Ž. Fuchs, 2009: The mechanics of gross moist stability. *J. Adv. Model. Earth Syst.*, **1** (9), doi:10.3894/JAMES.2009.1.9.

Riley Dellaripa, E. M., and E. D. Maloney, 2015: Analysis of MJO wind-flux feedbacks in the Indian Ocean using RAMA buoy observations. *J. Meteor. Soc. Japan*, **93A**, 1–20, doi:10.2151/jmsj.2015-021.

Sahany, S., J. D. Neelin, K. Hales, and R. B. Neale, 2012: Temperature–moisture dependence of the deep convective transition as a constraint on entrainment in climate models. *J. Atmos. Sci.*, **69**, 1340–1358, doi:10.1175/JAS-D-11-0164.1.

Schumacher, C., and R. A. Houze Jr., 2003: Stratiform rain in the tropics as seen by the TRMM Precipitation Radar. *J. Climate*, **16**, 1739–1756, doi:10.1175/1520-0442(2003)016<1739:SRITTA>2.0.CO;2.

Seo, K.-H., and W. Wang, 2010: The Madden–Julian oscillation simulated in the NCEP Climate Forecast System Model: The importance of stratiform heating. *J. Climate*, **23**, 4770–4793, doi:10.1175/2010JCLI2983.1.

Sobel, A., and E. D. Maloney, 2013: Moisture modes and the eastward propagation of the MJO. *J. Atmos. Sci.*, **70**, 187–192, doi:10.1175/JAS-D-12-0189.1.

——, J. Nilsson, and L. M. Polvani, 2001: The weak temperature gradient approximation and balanced tropical moisture waves. *J. Atmos. Sci.*, **58**, 3650–3665, doi:10.1175/1520-0469(2001)058<3650:TWTGAA>2.0.CO;2.

——, S. Wang, and D. Kim, 2014: Moist static energy budget of the MJO during DYNAMO. *J. Atmos. Sci.*, **71**, 4276–4291, doi:10.1175/JAS-D-14-0052.1.

Sugiyama, M., 2009: The moisture mode in the quasi-equilibrium tropical circulation model. Part I: Analysis based on the weak temperature gradient approximation. *J. Atmos. Sci.*, **66**, 1507–1523, doi:10.1175/2008JAS2690.1.

Takayabu, Y. N., S. Shige, W.-K. Tao, and N. Hirota, 2010: Shallow and deep latent heating modes over tropical oceans observed with TRMM PR spectral latent heating data. *J. Climate*, **23**, 2030–2046, doi:10.1175/2009JCLI3110.1.

Tseng, K.-C., C.-H. Sui, and T. Li, 2015: Moistening processes for Madden–Julian oscillations during DYNAMO/CINDY. *J. Climate*, **28**, 3041–3057, doi:10.1175/JCLI-D-14-00416.1.

Wimmers, A. J., and C. S. Velden, 2011: Seamless advective blending of total precipitable water retrievals from polar-orbiting satellites. *J. Appl. Meteor. Climatol.*, **50**, 1024–1036, doi:10.1175/2010JAMC2589.1.

Yanai, M., S. Esbensen, and J.-H. Chu, 1973: Determination of bulk properties of tropical cloud clusters from large-scale heat and moisture budgets. *J. Atmos. Sci.*, **30**, 611–627, doi:10.1175/1520-0469(1973)030<0611:DOBPOT>2.0.CO;2.

Yoneyama, K., C. Zhang, and C. N. Long, 2013: Tracking pulses of the Madden–Julian oscillation. *Bull. Amer. Meteor. Soc.*, **94**, 1871–1891, doi:10.1175/BAMS-D-12-00157.1.

Yu, L., and R. A. Weller, 2007: Objectively analyzed air–sea heat fluxes for the global ice-free oceans (1981–2005). *Bull. Amer. Meteor. Soc.*, **88**, 527–539, doi:10.1175/BAMS-88-4-527.

Zhang, C., 2005: Madden–Julian oscillation. *Rev. Geophys.*, **43**, RG2003, doi:10.1029/2004RG000158.

——, J. Gottschalck, E. D. Maloney, M. W. Moncrieff, F. Vitart, D. E. Waliser, B. Wang, and M. C. Wheeler, 2013: Cracking the MJO nut. *Geophys. Res. Lett.*, **40**, 1223–1230, doi:10.1002/grl.50244.

Zhang, M. H., J. L. Lin, R. T. Cederwall, J. J. Yio, and S. C. Xie, 1999: Sensitivity of the vertical velocity and advective tendencies analyzed over the ARM SGP site to input data and analysis methods. *Proc. Ninth ARM Science Team Meeting*, San Antonio, TX, ARM, 1–5. [Available online at https://www.arm.gov/publications/proceedings/conf09/extended_abs/zhang_mh.pdf.]

Brought to you by NOAA Central Library | Unauthenticated | Downloaded 08/13/24 01:21 PM UTC